

---

# CUTS+: High-dimensional Causal Discovery from Irregular Time-series

---

Yuxiao Cheng<sup>1\*</sup>   Lianglong Li<sup>1\*</sup>   Tingxiong Xiao<sup>1</sup>   Zongren Li<sup>3</sup>  
 Jinli Suo<sup>12†</sup>   Kunlun He<sup>3†</sup>   Qionghai Dai<sup>12†</sup>

<sup>1</sup>Department of Automation, Tsinghua University

<sup>2</sup>Institute for Brain and Cognitive Science, Tsinghua University (THUIBCS)

<sup>3</sup>Chinese PLA General Hospital

{cyx22,li-1119,xtx22}@mails.tsinghua.edu.cn

{lizongren,kunlunhe}@plagh.org   {jlsuo,qhdai}@tsinghua.edu.cn

## Abstract

Causal discovery in time-series is a fundamental problem in the machine learning community, enabling causal reasoning and decision-making in complex scenarios. Recently, researchers successfully discover causality by combining neural networks with Granger causality, but their performances degrade largely when encountering high-dimensional data because of the highly redundant network design and huge causal graphs. Moreover, the missing entries in the observations further hamper the causal structural learning. To overcome these limitations, We propose CUTS+, which is built on the Granger-causality-based causal discovery method CUTS and raises the scalability by introducing a technique called Coarse-to-fine-discovery (C2FD) and leveraging a message-passing-based graph neural network (MPGNN). Compared to previous methods on simulated, quasi-real, and real datasets, we show that CUTS+ largely improves the causal discovery performance on high-dimensional data with different types of irregular sampling.

## 1 Introduction

Analyzing complex interactions behind time-series, i.e., time-series analysis, is a fundamental problem in machine learning, and holds great potential in various real-world applications. However, the complex relationships buried under massive amounts of variables can be challenging for algorithm design. Recently, approaches have been proposed to extract causal relationships from observational data [46, 30, 24, 38, 8, 53]. This task is called time-series causal discovery, which can be regarded as a novel angle by enabling causal reasoning of time-series.

Although proven to efficiently discover causal relationships, most of these methods lack the ability to handle high-dimensional time-series. Actually, many causal discovery algorithms are only tested on datasets with fewer than 20 time-series (i.e.  $N \leq 20$ ) [46, 24], while the real time-series datasets often contain dozens or even hundreds of time-series, e.g., gene regulation networks or air quality index. Recently, Cheng et al. [8] proposed CUTS, an EM-Style approach to jointly perform causal graph learning and missing data imputation for irregular temporal data. Although CUTS proposed to boost causal discovery with data imputation and the other way around, the data prediction module is composed of component-wise LSTMs and MLPs with redundant structures and parameters, hampering the scalability when encountering high-dimensional datasets. Moreover, the causal graph in CUTS can be too large to learn with high accuracy.

---

\*Equal Contribution

†Corresponding author

To overcome these issues, we propose **CUTS+**, an extension of CUTS with scalability to high-dimensional time-series, via mutual boosting between scalable causal discovery and scalable time-series imputation. Our contributions include

- We propose CUTS+, an extension of CUTS [8] to largely increase scalability towards high-dimensional time-series.
- We specifically propose Coarse-to-fine-discovery (C2FD), a simple yet efficient technique to facilitate scalable causal graph optimization, and design a message-passing-based graph neural network (MPGNN) to avoid structural redundancy in CUTS+.
- With extensive experiments, we show that CUTS+ largely increases causal discovery performance, especially on high-dimensional datasets with multiple types of irregular sampling.

## 2 Related Works

**Causal Structural Learning / Causal Discovery.** Existing Causal Structural Learning (or Causal Discovery) approaches can be categorized into five classes. (i) *Constraint-based approaches*, such as PC[43], FCI[44], and PCMCI [38, 37, 14], build causal graphs by conditional independence tests. (ii) *Score-based learning algorithms* which include penalized Neural Ordinary Differential Equations and acyclicity constraint[2] [34]. (iii) *Convergent Cross Mapping (CCM)* proposed by Sugihara et al. [45] that reconstructs nonlinear state space for nonseparable weakly connected dynamic systems. This approach is later extended to situations of synchrony, confounding, or sporadic time series [54, 3, 5]. (iv) Approaches based on *Additive Noise Model (ANM)* that infer causal graph based on additive noise assumption [41, 21]. ANM is extended by Hoyer et al. [21] to nonlinear models with almost any nonlinearities. (v) *Granger-causality-based* approaches. Granger causality is initially proposed by Granger [18] who proposed to analyze the temporal causal relationships by testing the help of a time-series on predicting another time-series. Recently, Deep Neural Networks (NNs) are widely applied to infer nonlinear Granger causality since the central idea of Granger Causality is highly compatible with NNs. Researchers have successfully use Recurrent Neural Networks (RNNs) or other NNs for time series analysis to discover causal graphs [51, 46, 24, 30, 8]. This work also incorporates a deep neural network to discover Granger Causality.

**Scalable / High-dimensional Causal Discovery.** Scalability can be a serious problem when applying causal discovery algorithms to real data. With hundreds of time-series (or hundreds of static nodes), the potential possibility for causal relations grows exponentially. Existing approaches may fail because they involve either massive conditional independence tests [38], too many variables to be conditioned on [19], or large quantities of parameters to be optimized [46, 8]. To solve this problem, scalable or high-dimensional causal discovery approaches are proposed. In static settings, Hong et al. [19] and Morales-Alvarez et al. [33] propose to boost scalability via divide-and-conquer technique, Lopez et al. [29] limit the search space to low-rank factor graphs, Cundy et al. [11] instead leverages variational framework. In time-series settings like ours, the scalability issue is less explored. The most related work to ours is Xu et al. [53]’s which also uses Granger causality and simplifies the high-dimensional adjacency matrix with low-rank approximation. However, the low-rank assumption may not be satisfied in real scenarios. Our CUTS+ is an extension of Granger-causality-based approaches by alleviating the scalability issue without low-rank approximation.

## 3 Background

### 3.1 Time Series and Granger Causality

We inherit the notation in [8] and denote a uniformly sampled observation of a dynamic system as  $\mathbf{X} = \{\mathbf{x}_{i,1:T}\}_{i=1}^N$ , where  $x_{i,t}$  represents the  $i$ th time-series sampled at time point  $t$ , and  $t \in \{1, \dots, T\}$ ,  $i \in \{1, \dots, N\}$ , with  $T$  and  $N$  being the length and number of the time-series. Each sampled variable  $x_{i,t}$  is assumed to be generated by the following Structural Causal Model (SCM) with additive noise:

$$x_{i,t} = f_i(\mathbf{x}_{1,t-\tau:t-1}, \mathbf{x}_{2,t-\tau:t-1}, \dots, \mathbf{x}_{N,t-\tau:t-1}) + e_{i,t}, \quad i = 1, 2, \dots, N, \quad (1)$$

in which  $\tau$  denotes the maximal time lag. Our CUTS+ can also handle irregular time-series by jointly performing imputation and causal discovery. So to model the irregular time-series, a bi-value observation mask  $o_{t,i}$  is used to label the missing entries, i.e., the observed point equals the generated  $x_{i,t}$  when  $o_{t,i}$  equals to 1:  $\tilde{x}_{i,t} \triangleq x_{i,t} \cdot o_{t,i}$ . In this paper, we adopt the protocols of previous works [55, 10] and consider two types of data missing that often occur in practical observations:

- *Random Missing (RM)*. The data entries in the observations are missing with a certain probability  $p$ , here in our experiments the missing probability follows Bernoulli distribution  $o_{t,i} \sim \text{Ber}(1-p)$ .
- *Random Block Missing (RBM)*. Under a relatively small  $p$  for RM, we set a block failure probability  $p_{\text{blk}}$  and block length  $L_{\text{blk}} \sim \text{Uniform}(L_{\text{min}}, L_{\text{max}})$ , i.e. there exist  $p_{\text{blk}} \cdot N \cdot T$  missing blocks on average and each with length  $[L_{\text{min}}, L_{\text{max}}]$ .

In this work, we build on the Granger causality. Under the assumptions of no unobserved variables and no instantaneous effects, Peters et al. [35] provide justification of time-invariant Granger causality [30, 49]. For a dynamic system, time-series  $i$  Granger causes time-series  $j$  when the past values of time-series  $\mathbf{x}_i$  aid in the prediction of the current and future status of time-series  $\mathbf{x}_j$ . Specifically, time-series  $i$  Granger cause  $j$  if and only if there exists  $\mathbf{x}'_{i,t-\tau:t-1} \neq \mathbf{x}_{i,t-\tau:t-1}$  satisfying

$$f_j(\mathbf{x}_{1,t-\tau:t-1}, \dots, \mathbf{x}'_{i,t-\tau:t-1}, \dots, \mathbf{x}_{N,t-\tau:t-1}) \neq f_j(\mathbf{x}_{1,t-\tau:t-1}, \dots, \mathbf{x}_{i,t-\tau:t-1}, \dots, \mathbf{x}_{N,t-\tau:t-1}) \quad (2)$$

i.e., the past data points of time-series  $i$  influence the prediction of  $x_{j,t}$ . For simplicity, we use  $\mathbf{x}_i$  to denote  $\mathbf{x}_{i,t-\tau:t-1}$  in the following. The discovered pair-wise Granger causal relationship is a Directed Acyclic Graph (DAG), which is then represented with an adjacency matrix  $\mathbf{A} = \{a_{ij}\}_{i,j=1}^N$ , where  $a_{ij} = 1$  denotes time-series  $i$  Granger causes  $j$  and  $a_{ij} = 0$  means otherwise. The idea of Granger causality is highly compatible with the basic idea of neural networks (NNs) since NNs can serve as powerful predictors. In previous works, [8] prove that causal graph discovery in their CUTS converges to the true graphs under the Additive Noise Model and Universal Approximation Theorem for NNs, which again validates the successful combination of Granger causality and NNs.

### 3.2 Difficulties with High Dimensional Time-series

In real scenarios, it is common to face hundreds of long time-series with complex causal graphs. We now proceed to show difficulties when CUTS or other causal discovery algorithms handle such data.

**Large Adjacency Matrix.** The pairwise GC relationship, denoted as matrix  $\mathbf{A}_{N \times N}$ , can become very large as  $N$  increases. Prior works mainly focus on the settings when  $N \leq 20$  [46, 24, 8], and we show in the experiments that their performances degrade greatly when  $N > 20$ . Alternatively, Xu et al. [53] addresses the scalability issue at increasing data dimension via conducting low-rank approximation to the adjacency matrix, but the strong low-rank assumption of  $\mathbf{A}_{N \times N}$  does not hold in many scenarios.

**Redundancy of cMLP / cLSTM.** To uncover the black-box of NNs, Cheng et al. [8], Tank et al. [46] disentangle causal effects from causal parents to individual output series. As a result, one must use  $N$  separate MLPs/LSTMs to ensure the disentanglement. This is called component-wise MLP/LSTM (cMLP/cLSTM) and frequently used when discovering Granger causality [24]. In the following We formalize component-wise neural networks as ‘‘causally disentangled neural networks’’.

**Definition 1** Let  $\mathbf{x} \in \mathcal{X} \subset \mathbb{R}^n$ ,  $\mathbf{A} \in \mathcal{A} \subset \{0, 1\}^{n \times n}$  and  $\mathbf{y} \in \mathcal{Y} \subset \mathbb{R}^n$  be the input and output spaces. We say a neural network  $\mathbf{f}_\theta : \langle \mathcal{X}, \mathcal{A} \rangle \rightarrow \mathcal{Y}$  is a **causally disentangled neural network (CDNN)** if it has the form

$$\mathbf{f}_\theta(\mathbf{x}, \mathbf{A}) = [f_{\theta_1}(\mathbf{x} \odot \mathbf{a}_{:,1}), \dots, f_{\theta_n}(\mathbf{x} \odot \mathbf{a}_{:,n})]^T. \quad (3)$$

Here  $\mathbf{a}_{:,i}$  is the column vector of input causal adjacency matrix  $\mathbf{A}$ ;  $f_{\phi_j} : \mathcal{X}_j \rightarrow \mathcal{Y}_j$ , with  $\mathcal{X}_j \subset \mathbb{R}^n$  and  $\mathcal{Y}_j \subset \mathbb{R}$ ; the operator  $\odot$  denotes the Hadamard product.

Here the input to CDNN can also be  $\mathbf{X}$  with time dimension instead of  $\mathbf{x}$ , then  $\odot$  is defined as  $f_{\phi_j}(\mathbf{X} \odot \mathbf{a}_{:,j}) \triangleq f_{\phi_j}(\{\mathbf{x}_1 \cdot a_{1j}, \dots, \mathbf{x}_N \cdot a_{Nj}\})$ . Under this definition, Cheng et al. [8] proved that when approximating  $f_j$  with  $f_{\phi_j}$  (along with other assumptions), the discovered causal adjacency matrix will converge to the true Granger causal matrix. Although being a CDNN, cMLP / cLSTM consists of  $N$  separate networks and is highly redundant, because the shared dynamics among different time-series are modeled  $N$  times. This redundancy not only slows down the learning process but also degrades causal discovery accuracy. Therefore, the model does not scale well to high-dimension time-series. In the following section, we introduce two techniques to solve the scalability issue.

## 4 CUTS+

In this work, we implement the causal graph as Causal Probability Graph (CPGs)  $\tilde{\mathbf{M}}$  where the element  $m_{ij}$  represents the probability of time-series  $i$  Granger cause  $j$ , i.e.,  $m_{ij} = P(x_i \rightarrow x_j)$ . If  $\tilde{\mathbf{M}}_{ij}$  in the discovered graph  $\tilde{\mathbf{M}}$  is penalized to zero (or below some certain threshold), we can deduce that time-series  $i$  does not Granger cause  $j$ .

Similar to CUTS [8], we also adapts the EM-Style training strategy, and iteratively perform the **Causal Discovery Stage** and **Prediction Stage**. The overall learning process is illustrated in Fig. 1 and described in Section 4.3. To overcome the difficulties when encountering high-dimensional time-series, we propose to use coarse-to-fine discovery (C2FD) technique in the **Causal Discovery Stage** and message-passing neural network (MPNN) in the **Prediction Stage**.

#### 4.1 Coarse-to-fine Causal Discovery

To address the problem of **large adjacency matrix** discussed in Section 3.2, we propose Coarse-to-Fine causal Discovery (C2FD). Specifically, we split the time-series into several groups, i.e., time-series group  $\mathbf{X}_{\mathcal{G}_k} = \{\mathbf{x}_i\}_{i \in \mathcal{G}_k}$  where  $\mathcal{G}_k$  is the set of the indices within  $k$ th group, and  $k \in [1, N_g]$  with  $N_g$  being the group number. Each time-series is and can only be allocated to one group, i.e.,  $\forall k \neq l \in [1, N_g], \mathcal{G}_k \cap \mathcal{G}_l = \emptyset$ . The grouping is implemented with matrix decomposition of  $\tilde{\mathbf{M}}$ :

$$\tilde{\mathbf{M}} = \mathbf{G}^T \mathbf{Q} \quad (4)$$

where  $\mathbf{G} \in \mathbb{R}^{N_g \times N}$  is composed of entries  $g_{ki} = \begin{cases} 0, & \text{if } i \notin \mathcal{G}_k \\ 1, & \text{if } i \in \mathcal{G}_k \end{cases}$ . Since each time-series is and can

only be allocated to one group, the sum of each column vector of  $\mathbf{G}$  is 1, i.e.  $\forall i \in [1, N], \sum_{k=1}^{N_g} g_{ki} = 1$ . We define the Granger causality from group  $\mathbf{X}_{\mathcal{G}_k}$  as follows

**Definition 2** Group  $\mathbf{X}_{\mathcal{G}_k}$  Granger cause  $\mathbf{x}_j$  if there exists  $\mathbf{X}'_{\mathcal{G}_k} \neq \mathbf{X}_{\mathcal{G}_k}$ ,

$$f_j(\{\mathbf{X}'_{\mathcal{G}_k}, \mathbf{X} \setminus \mathbf{X}_{\mathcal{G}_k}\}) \neq f_j(\{\mathbf{X}_{\mathcal{G}_k}, \mathbf{X} \setminus \mathbf{X}_{\mathcal{G}_k}\}) \quad (5)$$

i.e., group  $\mathbf{x}_{\mathcal{G}_k}$  influence the prediction of  $x_{j,t}$ . Where  $\mathbf{X} \setminus \mathbf{X}_{\mathcal{G}_k} \triangleq \{\mathbf{x}_i\}_{i \notin \mathcal{G}_k}$ .

Then  $\mathbf{Q} \in \mathbb{R}^{N_g \times N}$  is the Group Causal Probability Graph (GCPG) with  $q_{ij} = P(\mathbf{X}_{\mathcal{G}_i} \rightarrow \mathbf{x}_j)$ .

**Initial Allocation.** Before training, we initiate  $\mathbf{G}$  with a relatively small  $N_g$  and consequently obtain a ‘‘coarse’’ grouping. Specifically, the time series are allocated into a group following

$$|\mathcal{G}_i| = \begin{cases} \lfloor N/N_g \rfloor, & \text{if } i \in [1, N_g - 1] \\ N - \lfloor N/N_g \rfloor \cdot (N_g - 1), & \text{if } i = N_g. \end{cases} \quad (6)$$

**Group Splitting.** During training, we periodically split each group into two groups, and then  $N_g$  is doubled every 20 epochs until every group contains only one time-series. Correspondingly, when doubling group numbers, GCPG element  $q_{ij}$  is allocated to 2 elements  $q_{i_1,j}$  and  $q_{i_2,j}$  in the new GCPG, as initial guesses. Here we assume a group Granger cause  $\mathbf{x}_j$  if at least one sub-group Granger cause  $\mathbf{x}_j$ , then  $q_{ij} = P(\mathbf{X}_{\mathcal{G}_i} \rightarrow \mathbf{x}_j) = 1 - P(\mathbf{X}_{\mathcal{G}_{i_1}} \nrightarrow \mathbf{x}_j)P(\mathbf{X}_{\mathcal{G}_{i_2}} \nrightarrow \mathbf{x}_j)$ . As initial guesses we assume  $P(\mathbf{X}_{\mathcal{G}_{i_1}} \rightarrow \mathbf{x}_j) = P(\mathbf{X}_{\mathcal{G}_{i_2}} \rightarrow \mathbf{x}_j)$ , then  $q_{i_1,j}$  and  $q_{i_2,j}$  are calculated as

$$q_{i_1,j} = q_{i_2,j} = 1 - \sqrt{1 - q_{ij}}. \quad (7)$$

**Convergence of C2FD.** We prove the convergence of C2FD with CDNN as predictor, with a similar manner to [8]. Due to space limit, we place the detailed assumptions, theorem, and proof in section A of the supplementary material.

The idea of coarse-to-fine is quite common in the field of machine learning [12, 39]. However, to our best knowledge, we are the first to introduce the idea into neural-network-based Granger causality. Actually, the advantage of introducing C2FD is two-fold. Firstly, the parameter number to learn is

Table 1: Nomenclature.

CPG	Causal Probability Graph $M$
GCPG	Group CPG $Q$
BCG	Binary Causal Graph $S$
MPNN	Message-Passing NN
MPGNN	Message-Passing GNN
C2FD	Coarse-to-fine Causal Discovery

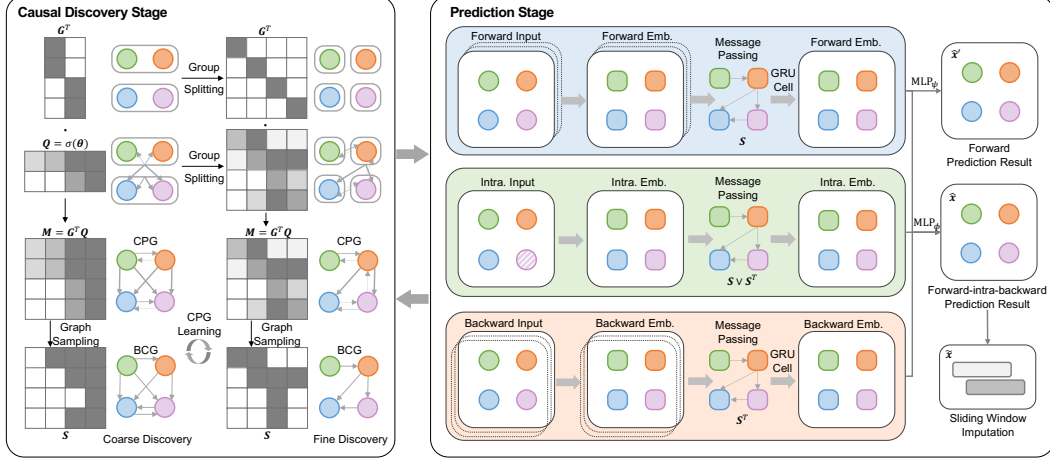


Figure 1: The architecture of CUTS+ with two alternative stages, both boosted for high-dimensional causal discovery. The **Causal Discovery Stage** is equipped with Coarse-to-fine Causal Discovery (C2FD) while the **Prediction Stage** is with Message-passing-based Graph Neural Network (MPGNN).

greatly decreased in the initial stages. In the initial stages when  $N_g \ll N$ , only  $N \cdot N_g$  instead of  $N^2$  parameters are required to be optimized. Secondly, the learning results with smaller  $N_g$  serve as initial guess for learning with larger  $N_g$ . When  $|\mathcal{G}_k| > 1$ , GCPG element  $q_{kj}$  increases towards 1 if at least one member Granger cause time-series  $j$ . Then the whole group is used to perform data prediction with higher accuracy. After doubling  $N_g$ , the optimizer further locates the sub-group that actually Granger causes  $j$ . The empirical advantage of C2FD is experimentally validated in Sec. 5.

## 4.2 Message-passing-based Graph Neural Network (MPGNN)

To satisfy the definition of **causal disentanglement** while preventing using highly-redundant cMLP / cLSTM, we leverage the Message-Passing Neural Network (MPNN [17]) for data prediction encoder. To learning the dynamics of the high-dimensional time-series, we alter the gated recurrent units (GRUs, [9]) by adding message passing layers. Firstly, we formulate single-layer MPNN as

$$\text{MPNN}_\nu(\mathbf{z}, \mathbf{h}'; \mathbf{s}) = \text{MLP}_\nu(\mathbf{h}', \mathbf{z} \odot \mathbf{s}) = \mathbf{h} \quad (8)$$

where  $\mathbf{h}'$  is the output of MPNN in the last layer,  $\text{MLP}_1(\cdot), \text{MLP}_2(\cdot)$  is multi-layer perceptrons (MLPs),  $\odot$  denotes the Hadamard product, and  $\mathbf{s} \in \{0, 1\}^N$  is the binary causal vector, i.e., a column in the sampled Binary Causal Graph (BCG, described in Section 4.3) where  $s_i = 1$  denotes  $z_i$  Granger cause the prediction. Similar to [10], we add MPNN to GRU units, which serves as a layer in MPGNN:

$$\mathbf{r}_t^j = \sigma \left( \text{MPNN}_{\nu_t^r} \left( \tilde{\mathbf{x}}_{:,t}, \mathbf{h}_{t-1}^j; \mathbf{s}_{:,j} \right) \right) \quad (9)$$

$$\mathbf{u}_t^j = \sigma \left( \text{MPNN}_{\nu_t^u} \left( \tilde{\mathbf{x}}_{:,t}, \mathbf{h}_{t-1}^j; \mathbf{s}_{:,j} \right) \right) \quad (10)$$

$$\mathbf{c}_t^j = \tanh \left( \text{MPNN}_{\nu_t^c} \left( \tilde{\mathbf{x}}_{:,t}, \mathbf{r}_t^j \odot \mathbf{h}_{t-1}^j; \mathbf{s}_{:,j} \right) \right) \quad (11)$$

$$\mathbf{h}_t^j = \mathbf{u}_t^j \odot \mathbf{h}_{t-1}^j + (1 - \mathbf{u}_t^j) \odot \mathbf{c}_t^j, \quad (12)$$

with  $\sigma(\cdot)$  being the sigmoid function. In the following we represent  $l$  MPGNN layers with  $\text{MPGNN}_\nu(\mathbf{X}, \mathbf{h}_0^j; \mathbf{s}_{:,j})$ , where  $\nu = \{\nu_1^r, \nu_1^u, \nu_1^c, \dots, \nu_l^r, \nu_l^u, \nu_l^c\}$  (parameters of MPNNs in all layers). Note that we share  $\nu$  for each  $j$ , which is the key to achieve scalability. After encoding with MPGNN, the prediction result  $\hat{x}_{j,t}$  is retrieved with a MLP decoder, i.e.,

$$\hat{x}_{j,t} = \text{MLP}_\psi \left( \mathbf{h}_{t-1}^j \right) \quad (13)$$

Our data imputation is performed with sliding windows (see supplementary material), where  $\tilde{\mathbf{x}}_{:,t}$  is the input data with its missing values filled with the prediction from the last windows. The imputation results is calculated as  $\tilde{x}_{j,t} = o_{j,t}x_{j,t} + (1 - o_{j,t})\hat{x}_{j,t}$ , which is used in the following sliding windows.

**Scalability of MPGNN.** The number of parameters needing to be optimized in MPGNN can be calculated with  $l(|\nu^r| + |\nu^u| + |\nu^c| + |\psi|)$ , where  $l$  is the number of MPGNN layers. Comparing CUTS+ with component-wise GRU, whose parameter number is  $Nl(|\nu^r| + |\nu^u| + |\nu^c| + |\psi|)$  (or cMLP / cLSTM [46] which is also  $O(Nl)$ ), the scalability is achieved by significantly reducing the number of optimization parameters. Since component-wise network-based prediction model is usually overparameterized and thus prone to overfitting [24], this design also help to reduce overfitting.

### 4.3 Overall Architecture

**Bernoulli Sampling of CPG.** Our CUTS+ represents causal relationships with CPG  $\tilde{\mathbf{M}}$ . To ensure elements of  $\tilde{\mathbf{M}}$  are within range  $[0, 1]$ , we set  $\mathbf{Q} = \sigma(\theta)$  where  $\theta$  is the parameter to learn and optimized with Gumbel-Softmax estimator [22]. CPG is then sampled to binary causal graph (BCG)  $\mathbf{S}$  where  $s_{ij} \sim \text{Ber}(m_{ij})$ . Finally BCG columns  $\mathbf{s}_{:,j}$  is used as adjacency matrix in MPNNs. Parameter  $\theta$  is optimized with Gumbel-Softmax estimator [22]. i.e.,

$$s_{\tau,ij} = \frac{\exp((\log(m_{\tau,ij}) + g)/\tau)}{\exp((\log(m_{\tau,ij}) + g)/\tau) + \exp((\log(1 - m_{\tau,ij}) + g)/\tau)}, \quad (14)$$

Where  $g = -\log(-\log(u))$ ,  $u \sim \text{Uniform}(0, 1)$ . We use a large  $\tau$  in the initial stages then decrease to a small value. This estimator has a relatively low variance, mimic Bernoulli distribution when  $\tau$  is small, and more importantly, enables continuous optimization of  $\mathbf{M}$ .

**Loss Functions.** CUTS+ iterates between *Causal Discovery Stage* and *Prediction Stage*. During the former stage, only the CPG  $\tilde{\mathbf{M}} = \sigma(\theta)$  will be optimized, so the optimization problem is

$$\max_{\theta} \mathcal{L}_{\text{graph}} = \max_{\theta} \frac{1}{NT} \sum_{j=1}^N \sum_{t=1}^T (\hat{x}_{j,t} - x_{j,t})^2 \cdot o_{j,t} + \lambda \|\sigma(\theta)\|_1. \quad (15)$$

In the latter stage, we only optimize the network parameters. Both the forward prediction and the forward-intra-backward prediction results are included:

$$\max_{\{\nu, \phi, \psi\}} \mathcal{L}_{\text{data}} = \max \frac{1}{NT} \sum_{j=1}^N \sum_{t=1}^{T_{\max}} (\hat{x}_{j,t} - x_{j,t})^2 \cdot o_{j,t}. \quad (16)$$

**Satisfaction of CDNN.** CDNN in Definition 1 is satisfied when a column of matrix  $\mathbf{A}$  only affect the corresponding component of prediction  $\mathbf{f}_{\theta}(x, \mathbf{A})$ . If we combine the prediction module  $\text{MPGNN}_{\nu}(\tilde{\mathbf{X}}, \mathbf{h}_0^j; \mathbf{s}_{:,j})$  with  $\text{MLP}_{\psi}(\cdot)$ , we get

$$\hat{x}'_{:,t} = \mathbf{f}_{\{\nu, \psi\}}(\mathbf{X}, \mathbf{S}) = \left[ \dots, \text{MLP}_{\psi} \left( \text{MPGNN}_{\nu} \left( \tilde{\mathbf{X}}, \mathbf{h}_0^j; \mathbf{s}_{:,j} \right) \right), \dots \right]^T \quad (17)$$

where  $\mathbf{h}_0^j$  is the initial value of GRU hidden states and irrelevant to  $\mathbf{x}$ . Therefore, our CUTS is a CDNN, and according to Theorem 1 in supplementary material Section A, the correct causal graph can be exactly recovered.

## 5 Experiments

In this section, we quantitatively evaluate the proposed CUTS+ and comprehensively compare it with state-of-the-art methods to validate our design.

**Baseline Algorithms.** To demonstrate its advantageous performance, we compared CUTS+ with 7 baseline algorithms: (i) Neural Granger Causality (NGC, [46]), which utilizes MLPs and LSTMs to infer Granger causal relationships; (ii) economy-SRU (eSRU, [24]), a variant of SRU that is less prone to over-fitting when inferring Granger causality; (iii) PCMCI [38], a non-Granger-causality-based method that uses conditional independence tests; (iv) Latent Convergent Cross Mapping (LCCM, [5]), a CCM-based approach that also tackles the irregular time-series problem; (v) Neural Graphical Model (NGM, [2]), which uses Neural Ordinary Differential Equations (Neural-ODE) to handle irregular time-series data; (vi) Scalable Causal Graph Learning (SCGL, [53]) that address scalable causal discovery problem with low-rank assumption; and (vii) CUTS [8]. We evaluated the

Table 2: Performance comparison of CUTS+ with NGC, eSRU, NGM, SCGL, and CUTS combined with ZOH and TimesNet for imputation. Note that we do not perform experiments with PCMCI and LCCM, because with a large  $N$  the running times for these two methods are extremely long. Comparisons to PCMCI and LCCM are performed on NetSim and Dream-3 datasets (Tab. 3).

Met.	Imput.	VAR with RM ( $N = 128$ )		VAR with RBM ( $N = 128$ )	
		$p = 0.3$	$p = 0.6$	$p_{\text{blk}} = 0.15\%$	$p_{\text{blk}} = 0.3\%$
NGC	ZOH	0.8234 $\pm$ 0.0082	0.7419 $\pm$ 0.0056	0.8638 $\pm$ 0.0165	0.8357 $\pm$ 0.0161
	TimesNet	0.7900 $\pm$ 0.0111	0.6560 $\pm$ 0.0112	0.8519 $\pm$ 0.0056	0.8292 $\pm$ 0.0083
eSRU	ZOH	0.6627 $\pm$ 0.0071	0.6711 $\pm$ 0.0097	0.6606 $\pm$ 0.0152	0.6457 $\pm$ 0.0060
	TimesNet	0.6175 $\pm$ 0.0149	0.5671 $\pm$ 0.0156	0.6643 $\pm$ 0.0097	0.6488 $\pm$ 0.0096
SCGL	ZOH	0.6627 $\pm$ 0.0071	0.6711 $\pm$ 0.0097	0.6606 $\pm$ 0.0152	0.6457 $\pm$ 0.0060
	TimesNet	0.6536 $\pm$ 0.0180	0.6542 $\pm$ 0.0048	0.6558 $\pm$ 0.0118	0.6631 $\pm$ 0.0138
	NGM	0.5815 $\pm$ 0.0494	0.5016 $\pm$ 0.0010	0.5918 $\pm$ 0.0700	0.5003 $\pm$ 0.0004
CUTS		0.9434 $\pm$ 0.0123	0.8814 $\pm$ 0.0151	0.9579 $\pm$ 0.0085	0.9505 $\pm$ 0.0091
CUTS w C2FD		0.9594 $\pm$ 0.0094	0.8752 $\pm$ 0.0183	0.9742 $\pm$ 0.0061	0.9651 $\pm$ 0.0072
CUTS+		<b>0.9923 <math>\pm</math> 0.0030</b>	<b>0.9876 <math>\pm</math> 0.0034</b>	<b>0.9927 <math>\pm</math> 0.0029</b>	<b>0.9919 <math>\pm</math> 0.0032</b>

Met.	Imput.	Lorenz-96 with RM ( $N = 256$ )		Lorenz-96 with RBM ( $N = 256$ )	
		$p = 0.3$	$p = 0.6$	$p_{\text{blk}} = 0.15\%$	$p_{\text{blk}} = 0.3\%$
NGC	ZOH	0.9755 $\pm$ 0.0092	0.8469 $\pm$ 0.0331	0.9893 $\pm$ 0.0022	0.9760 $\pm$ 0.0042
	TimesNet	0.9415 $\pm$ 0.0183	0.5000 $\pm$ 0.0000	0.9685 $\pm$ 0.0070	0.7965 $\pm$ 0.0442
eSRU	ZOH	0.9735 $\pm$ 0.0019	0.8972 $\pm$ 0.0046	0.9821 $\pm$ 0.0019	0.9728 $\pm$ 0.0016
	TimesNet	0.9618 $\pm$ 0.0044	0.8742 $\pm$ 0.0047	0.9794 $\pm$ 0.0042	0.9762 $\pm$ 0.0033
SCGL	ZOH	0.6191 $\pm$ 0.0090	0.5182 $\pm$ 0.0109	0.6308 $\pm$ 0.0061	0.6195 $\pm$ 0.0069
	TimesNet	0.6210 $\pm$ 0.0032	0.5280 $\pm$ 0.0060	0.6312 $\pm$ 0.0072	0.6054 $\pm$ 0.0034
NGM		0.9620 $\pm$ 0.0072	0.6125 $\pm$ 0.0372	0.9831 $\pm$ 0.0031	0.9866 $\pm$ 0.0006
CUTS		0.9360 $\pm$ 0.0043	0.8668 $\pm$ 0.0043	0.9430 $\pm$ 0.0030	0.9330 $\pm$ 0.0053
CUTS w C2FD		0.9790 $\pm$ 0.0016	0.9069 $\pm$ 0.0036	0.9874 $\pm$ 0.0009	0.9834 $\pm$ 0.0015
CUTS+		<b>0.9954 <math>\pm</math> 0.0006</b>	<b>0.9734 <math>\pm</math> 0.0169</b>	<b>0.9967 <math>\pm</math> 0.0001</b>	<b>0.9966 <math>\pm</math> 0.0002</b>

performance in terms of the area under the ROC curve (AUROC) criterion. For a fair comparison, we search the best hyperparameters for the baseline algorithms on the validation dataset, and test performances on testing sets for 5 random seeds per experiment. For the baseline algorithms that could not handle irregular time-series data, i.e., NGC, PCMCI, SCGL, and eSRU, we imputed the irregular time-series using two algorithms: Zero-order Holder (ZOH, filling with the nearest historical sample, does not introduce future samples), and state-of-the-art imputation algorithm TimesNet [52].

**Ablation Study Settings.** Our main technical contributions are introducing C2FD and MPGNN into causal discovery. To quantitatively validate these two techniques, we add C2FD into the original CUTS [8] to get ‘‘CUTS w C2FD’’, measure C2FD’s performance gain by comparing ‘‘CUTS’’ with ‘‘CUTS w C2FD’’ and verify MPGNN by comparing ‘‘CUTS w C2FD’’ with ‘‘CUTS+’’.

**Datasets.** We assess the performance of the causal discovery approach CUTS+ on three types of datasets: simulated data, quasi-realistic data (i.e., synthesized under physically meaningful causality), and real data. Simulated datasets include linear Vector Autoregressive (VAR) and nonlinear Lorenz-96 models [23], quasi-realistic data are from NetSim [42] and Dream-3 [36], while real datasets include Air Quality datasets from 163 monitor stations across 20 Chinese cities. Irregular observations are generated via Random Missing (RM) and Random Block Missing (RBM). For statistical evaluation of causal discovery algorithms, we average over results on simulations from different random seeds.

## 5.1 Results on Simulated Datasets

**VAR.** VAR datasets are simulated with the linear equation  $\mathbf{x}_{:,t} = \sum_{\tau=1}^{\tau_{max}} \mathbf{A}\mathbf{x}_{:,t-\tau} + \mathbf{e}_{:,t}$ , where the matrix  $\mathbf{A}$  is the causal coefficients and  $\mathbf{e}_{:,t} \sim \mathcal{N}(\mathbf{0}, \sigma\mathbf{I})$ . Time-series  $i$  Granger cause time-series  $j$  if  $a_{ij} > 0$ . The objective of causal discovery is to find the non-zero elements in causal graph  $\mathbf{A}$  with  $\hat{\mathbf{M}}$ . We set  $\tau_{max} = 3$  and time-series length  $L = 1000$  in this experiment. One can observe in Tab. 6 that CUTS+ beats all other algorithms with a clear margin.

**Lorenz-96.** Lorenz-96 datasets are simulated according to  $\frac{dx_{i,t}}{dt} = -x_{i-1,t}(x_{i-2,t} - x_{i+1,t}) - x_{i,t} + F$ , where we set  $F = 10$ ,  $L = 1000$ . In this model each time-series  $\mathbf{x}_i$  is affected by historical values of four time-series  $\mathbf{x}_{i-2}$ ,  $\mathbf{x}_{i-1}$ ,  $\mathbf{x}_i$ ,  $\mathbf{x}_{i+1}$ , and each row in the true causal graph  $\mathbf{A}$  has four non-zero elements. Tab. 6 shows that CUTS+ is advantageous over other algorithms. By comparing

Table 3: Performance comparison of CUTS+ with PCMCI, NGC, eSRU, NGM, SCGL, LCCM and CUTS, combined with ZOH and TimesNet for imputation.

Met.	Imput.	NetSim with RM ( $N = 15$ )		Imput.	Dream-3 ( $N = 100$ )
		$p = 0.1$	$p = 0.2$		
PCMCI	ZOH	0.7625 $\pm$ 0.0539	0.7455 $\pm$ 0.0675	w/o	0.5517 $\pm$ 0.0261
	TimesNet	0.7766 $\pm$ 0.0640	0.7553 $\pm$ 0.0267		
NGC	ZOH	0.7656 $\pm$ 0.0576	0.7668 $\pm$ 0.0403	w/o	0.5579 $\pm$ 0.0313
	TimesNet	0.6774 $\pm$ 0.0788	0.6154 $\pm$ 0.0787		
eSRU	ZOH	0.6384 $\pm$ 0.0473	0.6592 $\pm$ 0.0248	w/o	0.5587 $\pm$ 0.0335
	TimesNet	0.6684 $\pm$ 0.0367	0.6367 $\pm$ 0.0481		
SCGL	ZOH	0.7278 $\pm$ 0.0253	0.7301 $\pm$ 0.0277	w/o	0.5273 $\pm$ 0.0276
	TimesNet	0.6905 $\pm$ 0.0193	0.7062 $\pm$ 0.0228		
LCCM	w/o	0.7711 $\pm$ 0.0301	0.7594 $\pm$ 0.0246	w/o	0.5046 $\pm$ 0.0318
NGM	w/o	0.7417 $\pm$ 0.0380	0.7215 $\pm$ 0.0330	w/o	0.5477 $\pm$ 0.0252
CUTS	w/o	0.7948 $\pm$ 0.0381	0.7699 $\pm$ 0.0550	w/o	0.5915 $\pm$ 0.0344
CUTS w C2FD	w/o	— ( $N$ too small for C2FD)		w/o	<b>0.6123 <math>\pm</math> 0.0497</b>
<b>CUTS+</b>	w/o	<b>0.8671 <math>\pm</math> 0.0192</b>	<b>0.8361 <math>\pm</math> 0.0256</b>	w/o	<b>0.6150 <math>\pm</math> 0.0949</b>

“CUTS”, “CUTS w C2FD”, and “CUTS+”, we see that both C2FD and MPGNN contribute to the performance gain. C2FD is relatively more helpful on Lorenz-96, and MPGNN helps more on VAR.

**Scalability.** The VAR and Lorenz-96 datasets support setting  $N$ . To demonstrate CUTS+’s scalability to high dimensional data, we compare CUTS+ with the two best-performing algorithms, i.e., CUTS and NGC (combining ZOH). We set causal parents for each time-series in VAR are the same when  $N$  changes. By increasing the time series length  $N$  of VAR and Lorenz-96 datasets, we observe that AUROC of CUTS and NGC degrades significantly when  $N$  increases on both datasets. On the contrary, CUTS+ beats both algorithms with a clear margin, and the advantages are especially prominent with a large  $N$ . The time costs for 32, 128, and 512 time-series are 25 min, 28 min, and 36 min, respectively. More experiments on scalability are shown in supplementary material Section B.

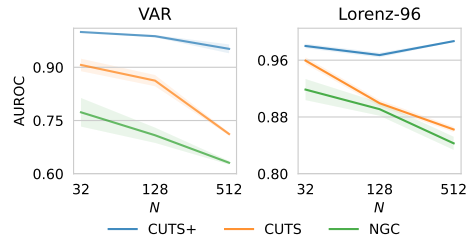


Figure 2: Comparison of scalability with CUTS and NGC in terms of AUROC (RM with  $p = 0.6$ ).

## 5.2 Quasi-Realistic Datasets

**NetSim.** To validate CUTS+’s performance on scenarios with physical meaning, We use data from 5 humans in NetSim datasets, which are generated with synthesized dynamics of brain region connectivity<sup>3</sup>. The total length of each time-series data  $T = 200$  and the number of time-series  $N = 15$ . Since  $T$  is relatively small, we do experiments on RM only with mild missingness ( $p = 0.1$  and  $0.2$ ). Since  $N$  is small, we do not perform C2FD. The results in Tab. 3 show that CUTS+ beats all other methods, which proves that our approach can also handle regular-dimensional data and shorter time-series. The ablation also shows prominent performance gain with MPGNN.

**Dream-3.** Dream-3 [36] is a gene expression and regulation dataset widely used as causal discovery benchmarks [24, 46]. This dataset contains 5 models, each representing measurements of 100 gene expression levels. The length of each measured trajectory is  $T = 21$ , which is too short to perform RM or RBM, so we only compare with baselines for regular time-series on Dream-3. The results are listed in Tab. 3, which shows that our CUTS+ performs better than the others, proving that our approach can also handle data without missing entries. As for the ablation study, we observe that C2FD contributes much more than MPGNN on this data. This is attributed to the fact that short series do not benefit a lot from MPGNN and large time-series number  $N = 100$  makes extensive use of C2FD’s advantages.

## 5.3 Real Datasets

**Air Quality (AQI).** We test our CUTS+ on AQI, a real high-dimensional dataset with  $N = 163$ ,  $T = 8760$ . We do not have access to the ground-truth causal graph because of the extremely

<sup>3</sup>Shared at <https://www.fmrib.ox.ac.uk/datasets/netsim/sims.tar.gz>

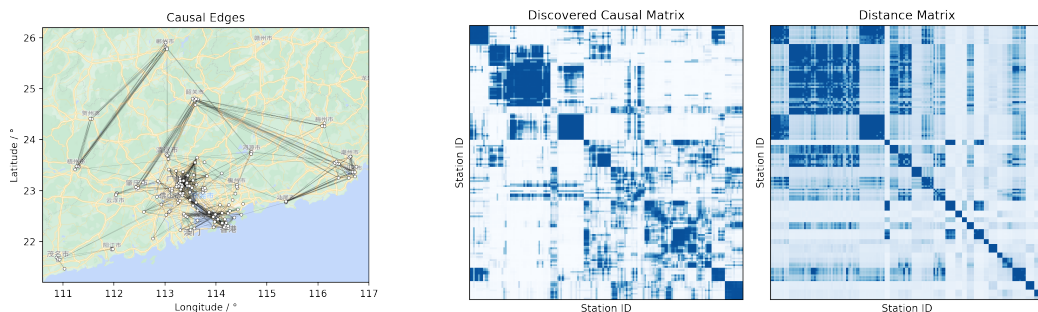


Figure 3: Causal discovery results on AQI dataset (left: plot overlaid on the map; middle: matrix visualization), and comparison with the distance matrix might indicating the true causal graph (right).

complex atmosphere physics, so quantitative performance evaluation and comparisons with baselines are inapplicable. However, we have a prior that the real causal relationships are very closely related to the geometrical distances. Therefore, to verify the causal discovery results of CUTS+, we compare the discovered CPG  $\tilde{M}$  (Fig. 3 middle) with the distance matrix  $\mathbf{D}$  (where  $d_{ij} \propto 1/\text{dist}(i, j)$ , Fig. 3 right). It can be observed that the discovered causal matrix does mimic the distance matrix. We also plot the CPG edges with  $P(i \rightarrow j) > 0.95$  on the map (Fig. 3 left), which shows that most discovered causal edges connect stations not far apart. This indirectly demonstrates the effectiveness of CUTS+ on real high-dimensional data.

#### 5.4 Additional Information

The assumptions, theorems, and proof for convergence of CPG when performing C2FD is provided in Supplementary Materials **Section A**. Our CUTS+ performs imputation and causal discovery jointly, and as a result accurate imputation is crucial for reliable causal discovery. So in **Section B**, we perform quantitative experiments on imputation. We also provide a brief literature review on time-series imputation algorithms and compare our CUTS+ to these approaches in terms of MSE and MAPE metrics. Other supplementary experiments are also included. We provide implementation details for CUTS in **Section C**, including network structure, hyper-parameters for each experiments, configuration for RM and RBM, and detailed settings for baseline algorithms. Additionally, we list the broader impacts and limitations in **Section D and E**.

## 6 Conclusions

We propose CUTS+, a Granger-causality-based causal discovery approach, to handle high-dimensional time-series with irregular sampling. We largely improve the scalability with respect to the data dimension by (a) introducing Coarse-to-fine Discovery (C2FD) to resolve the large CPG problem and (b) designing a Message-passing-based Graph Neural Network (MPGNN) to address the redundant network parameters problem. Comparing to previous approaches, CUTS+ largely increases AUROC especially when confronted with high dimensional time series. Our future works include: (i) High-dimensional causal discovery with latent confounder or instantaneous effect. (ii) Explaining neural network with causal models. Our code will soon be publicly available at <https://github.com/jarrycyx/unnc>.

## Acknowledgments and Disclosure of Funding

This work is jointly funded by Ministry of Science and Technology of China (Grant No. 2020AAA0108202), National Natural Science Foundation of China (Grant No. 61931012 and 62088102), Beijing Natural Science Foundation (Grant No. Z200021), and Project of Medical Engineering Laboratory of Chinese PLA General Hospital (Grant No. 2022SYSZZKY21).

## References

- [1] Melissa J. Azur, Elizabeth A. Stuart, Constantine Frangakis, and Philip J. Leaf. Multiple imputation by chained equations: What is it and how does it work? *International Journal of Methods in Psychiatric Research*, 20(1):40–49, 2011. ISSN 1557-0657. doi: 10.1002/mpr.329.

- [2] Alexis Bellot, Kim Branson, and Mihaela van der Schaar. Neural graphical modelling in continuous-time: Consistency guarantees and algorithms. In *International Conference on Learning Representations*, February 2022.
- [3] Zsigmond Benkő, Ádám Zlatniczki, Marcell Stippinger, Dániel Fabó, András Sólyom, Loránd Erőss, András Telcs, and Zoltán Somogyvári. Complete Inference of Causal Relations between Dynamical Systems, February 2020.
- [4] Lorenzo Beretta and Alessandro Santaniello. Nearest neighbor imputation algorithms: A critical evaluation. *BMC Medical Informatics and Decision Making*, 16(3):74, July 2016. ISSN 1472-6947. doi: 10.1186/s12911-016-0318-z.
- [5] Edward De Brouwer, Adam Arany, Jaak Simm, and Yves Moreau. Latent Convergent Cross Mapping. In *International Conference on Learning Representations*, March 2021.
- [6] Wei Cao, Dong Wang, Jian Li, Hao Zhou, Lei Li, and Yitan Li. BRITS: Bidirectional recurrent imputation for time series. In *Advances in Neural Information Processing Systems*, volume 31. Curran Associates, Inc., 2018.
- [7] Zhengping Che, Sanjay Purushotham, Kyunghyun Cho, David Sontag, and Yan Liu. Recurrent neural networks for multivariate time series with missing values. *Scientific reports*, 8(1):1–12, 2018.
- [8] Yuxiao Cheng, Runzhao Yang, Tingxiong Xiao, Zongren Li, Jinli Suo, Kunlun He, and Qionghai Dai. CUTS: Neural Causal Discovery from Irregular Time-Series Data. In *The Eleventh International Conference on Learning Representations*, February 2023.
- [9] Kyunghyun Cho, Bart van Merriënboer, Caglar Gulcehre, Dzmitry Bahdanau, Fethi Bougares, Holger Schwenk, and Yoshua Bengio. Learning Phrase Representations using RNN Encoder-Decoder for Statistical Machine Translation, September 2014.
- [10] Andrea Cini, Ivan Marisca, and Cesare Alippi. Filling the Gaps: Multivariate time series imputation by graph neural networks. In *International Conference on Learning Representations*, February 2022.
- [11] Chris Cundy, Aditya Grover, and Stefano Ermon. BCD Nets: Scalable Variational Approaches for Bayesian Causal Discovery. In *Advances in Neural Information Processing Systems*, volume 34, pages 7095–7110. Curran Associates, Inc., 2021.
- [12] Francois Fleuret and Donald Geman. Coarse-to-Fine Face Detection. *International Journal of Computer Vision*, 41(1):85–107, January 2001. ISSN 1573-1405. doi: 10.1023/A:1011113216584.
- [13] David Fung. Methods for the estimation of missing values in time series. *Theses: Doctorates and Masters*, January 2006.
- [14] Andreas Gerhardus and Jakob Runge. High-recall causal discovery for autocorrelated time series with latent confounders. In *Advances in Neural Information Processing Systems*, volume 33, pages 12615–12625. Curran Associates, Inc., 2020.
- [15] Jonathan Gillard and Konstantin Usevich. Hankel low-rank approximation and completion in time series analysis and forecasting: A brief review, June 2022.
- [16] Jonathan Gillard and Anatoly Zhigljavsky. Application of structured low-rank approximation methods for imputing missing values in time series. *Statistics and Its Interface*, 8(3):321–330, 2015. ISSN 1938-7997. doi: 10.4310/SII.2015.v8.n3.a6.
- [17] Justin Gilmer, Samuel S. Schoenholz, Patrick F. Riley, Oriol Vinyals, and George E. Dahl. Neural Message Passing for Quantum Chemistry. In *Proceedings of the 34th International Conference on Machine Learning*, pages 1263–1272. PMLR, July 2017.
- [18] C. W. J. Granger. Investigating causal relations by econometric models and cross-spectral methods. *Econometrica*, 37(3):424–438, 1969. ISSN 0012-9682. doi: 10.2307/1912791.
- [19] Yinghan Hong, Zhusong Liu, and Guizhen Mai. An efficient algorithm for large-scale causal discovery. *Soft Computing*, 21(24):7381–7391, December 2017. ISSN 1433-7479. doi: 10.1007/s00500-016-2281-0.
- [20] Kurt Hornik, Maxwell Stinchcombe, and Halbert White. Multilayer feedforward networks are universal approximators. *Neural networks*, 2(5):359–366, 1989.
- [21] Patrik Hoyer, Dominik Janzing, Joris M Mooij, Jonas Peters, and Bernhard Schölkopf. Nonlinear causal discovery with additive noise models. In *Advances in Neural Information Processing Systems*, volume 21. Curran Associates, Inc., 2008.

- [22] Eric Jang, Shixiang Gu, and Ben Poole. Categorical reparameterization with gumbel-softmax. November 2016. doi: 10.48550/arXiv.1611.01144.
- [23] A. Karimi and M. R. Paul. Extensive chaos in the lorenz-96 model. *Chaos: An Interdisciplinary Journal of Nonlinear Science*, 20(4):043105, December 2010. ISSN 1054-1500. doi: 10.1063/1.3496397.
- [24] Saurabh Khanna and Vincent Y. F. Tan. Economy statistical recurrent units for inferring nonlinear granger causality. In *International Conference on Learning Representations*, March 2020.
- [25] Sanmukh R. Kuppannagari, Yao Fu, Chung Ming Chueng, and Viktor K. Prasanna. Spatio-Temporal Missing Data Imputation for Smart Power Grids. In *Proceedings of the Twelfth ACM International Conference on Future Energy Systems, E-Energy '21*, pages 458–465, New York, NY, USA, June 2021. Association for Computing Machinery. ISBN 978-1-4503-8333-2. doi: 10.1145/3447555.3466586.
- [26] Linchao Li, Jian Zhang, Yonggang Wang, and Bin Ran. Missing Value Imputation for Traffic-Related Time Series Data Based on a Multi-View Learning Method. *IEEE Transactions on Intelligent Transportation Systems*, 20(8):2933–2943, August 2019. ISSN 1558-0016. doi: 10.1109/TITS.2018.2869768.
- [27] Zachary C. Lipton, David Kale, and Randall Wetzel. Directly Modeling Missing Data in Sequences with RNNs: Improved Classification of Clinical Time Series. In *Proceedings of the 1st Machine Learning for Healthcare Conference*, pages 253–270. PMLR, December 2016.
- [28] Caizheng Liu, Guangfan Cui, and Shenghua Liu. CGCNImp: A causal graph convolutional network for multivariate time series imputation. *PeerJ Computer Science*, 8:e966, April 2022. ISSN 2376-5992. doi: 10.7717/peerj-cs.966.
- [29] Romain Lopez, Jan-Christian Huetter, Jonathan Pritchard, and Aviv Regev. Large-Scale Differentiable Causal Discovery of Factor Graphs. *Advances in Neural Information Processing Systems*, 35:19290–19303, December 2022.
- [30] Sindy Löwe, David Madras, Richard Zemel, and Max Welling. Amortized causal discovery: Learning to infer causal graphs from time-series data. In *Proceedings of the First Conference on Causal Learning and Reasoning*, pages 509–525. PMLR, June 2022.
- [31] Yonghong Luo, Xiangrui Cai, Ying ZHANG, Jun Xu, and Yuan xiaojie. Multivariate Time Series Imputation with Generative Adversarial Networks. In *Advances in Neural Information Processing Systems*, volume 31. Curran Associates, Inc., 2018.
- [32] Rahul Mazumder, Trevor Hastie, and Robert Tibshirani. Spectral Regularization Algorithms for Learning Large Incomplete Matrices. *Journal of Machine Learning Research*, 11(80):2287–2322, 2010. ISSN 1533-7928.
- [33] Pablo Morales-Alvarez, Wenbo Gong, Angus Lamb, Simon Woodhead, Simon Peyton Jones, Nick Pawlowski, Miltiadis Allamanis, and Cheng Zhang. Simultaneous Missing Value Imputation and Structure Learning with Groups. *Advances in Neural Information Processing Systems*, 35:20011–20024, December 2022.
- [34] Roxana Pamfil, Nisara Sriwattanaworachai, Shaan Desai, Philip Pilgerstorfer, Konstantinos Georgatzis, Paul Beaumont, and Bryon Aragam. DYNOTEARS: Structure learning from time-series data. In *Proceedings of the Twenty Third International Conference on Artificial Intelligence and Statistics*, pages 1595–1605. PMLR, June 2020.
- [35] Jonas Peters, Dominik Janzing, and Bernhard Schölkopf. *Elements of Causal Inference: Foundations and Learning Algorithms*. The MIT Press, 2017. ISBN 978-0-262-03731-0 978-0-262-34429-6.
- [36] Robert J. Prill, Daniel Marbach, Julio Saez-Rodriguez, Peter K. Sorger, Leonidas G. Alexopoulos, Xiaowei Xue, Neil D. Clarke, Gregoire Altan-Bonnet, and Gustavo Stolovitzky. Towards a Rigorous Assessment of Systems Biology Models: The DREAM3 Challenges. *PLOS ONE*, 5(2):e9202, 2010. ISSN 1932-6203. doi: 10.1371/journal.pone.0009202.
- [37] Jakob Runge. Discovering contemporaneous and lagged causal relations in autocorrelated nonlinear time series datasets. In *Proceedings of the 36th Conference on Uncertainty in Artificial Intelligence (UAI)*, pages 1388–1397. PMLR, August 2020.
- [38] Jakob Runge, Peer Nowack, Marlene Kretschmer, Seth Flaxman, and Dino Sejdinovic. Detecting and quantifying causal associations in large nonlinear time series datasets. *Science Advances*, 5(11):eaau4996. doi: 10.1126/sciadv.aau4996.

- [39] Paul-Edouard Sarlin, Cesar Cadena, Roland Siegwart, and Marcin Dymczyk. From Coarse to Fine: Robust Hierarchical Localization at Large Scale. In *Proceedings of the IEEE/CVF Conference on Computer Vision and Pattern Recognition*, pages 12716–12725, 2019.
- [40] Lifeng Shen, Qianli Ma, and Sen Li. End-to-End Time Series Imputation via Residual Short Paths. In *Proceedings of The 10th Asian Conference on Machine Learning*, pages 248–263. PMLR, November 2018.
- [41] Shohei Shimizu, Patrik O. Hoyer, Aapo Hyv&#228, rinen, and Antti Kerminen. A Linear Non-Gaussian Acyclic Model for Causal Discovery. *Journal of Machine Learning Research*, 7(72):2003–2030, 2006. ISSN 1533-7928.
- [42] Stephen M. Smith, Karla L. Miller, Gholamreza Salimi-Khorshidi, Matthew Webster, Christian F. Beckmann, Thomas E. Nichols, Joseph D. Ramsey, and Mark W. Woolrich. Network modelling methods for fMRI. *NeuroImage*, 54(2):875–891, January 2011. ISSN 1053-8119. doi: 10.1016/j.neuroimage.2010.08.063.
- [43] Peter Spirtes and Clark Glymour. An algorithm for fast recovery of sparse causal graphs. *Social science computer review*, 9(1):62–72, 1991.
- [44] Peter Spirtes, Clark N. Glymour, Richard Scheines, and David Heckerman. *Causation, Prediction, and Search*. MIT press, 2000.
- [45] George Sugihara, Robert May, Hao Ye, Chih-hao Hsieh, Ethan Deyle, Michael Fogarty, and Stephan Munch. Detecting Causality in Complex Ecosystems. *Science*, 338(6106):496–500, October 2012. doi: 10.1126/science.1227079.
- [46] Alex Tank, Ian Covert, Nicholas Foti, Ali Shojaie, and Emily B. Fox. Neural granger causality. *IEEE Transactions on Pattern Analysis and Machine Intelligence*, 44(8):4267–4279, 2022. ISSN 1939-3539. doi: 10.1109/TPAMI.2021.3065601.
- [47] Olga Troyanskaya, Michael Cantor, Gavin Sherlock, Pat Brown, Trevor Hastie, Robert Tibshirani, David Botstein, and Russ B. Altman. Missing value estimation methods for DNA microarrays. *Bioinformatics*, 17(6):520–525, June 2001. ISSN 1367-4803. doi: 10.1093/bioinformatics/17.6.520.
- [48] Stef Van Buuren and Karin Groothuis-Oudshoorn. Mice: Multivariate imputation by chained equations in R. *Journal of statistical software*, 45:1–67, 2011.
- [49] Matthew J. Vowels, Necati Cihan Camgoz, and Richard Bowden. D’ya like dags? A survey on structure learning and causal discovery, March 2021.
- [50] Ian R. White, Patrick Royston, and Angela M. Wood. Multiple imputation using chained equations: Issues and guidance for practice. *Statistics in medicine*, 30(4):377–399, 2011.
- [51] Alexander P. Wu, Rohit Singh, and Bonnie Berger. Granger causal inference on dags identifies genomic loci regulating transcription. In *International Conference on Learning Representations*, March 2022.
- [52] Haixu Wu, Tengge Hu, Yong Liu, Hang Zhou, Jianmin Wang, and Mingsheng Long. TimesNet: Temporal 2D-Variation Modeling for General Time Series Analysis. In *The Eleventh International Conference on Learning Representations*, February 2023.
- [53] Chenxiao Xu, Hao Huang, and Shinjae Yoo. Scalable Causal Graph Learning through a Deep Neural Network. In *Proceedings of the 28th ACM International Conference on Information and Knowledge Management, CIKM ’19*, pages 1853–1862, New York, NY, USA, November 2019. Association for Computing Machinery. ISBN 978-1-4503-6976-3. doi: 10.1145/3357384.3357864.
- [54] Hao Ye, Ethan R. Deyle, Luis J. Gilarranz, and George Sugihara. Distinguishing time-delayed causal interactions using convergent cross mapping. *Scientific Reports*, 5(1):14750, October 2015. ISSN 2045-2322. doi: 10.1038/srep14750.
- [55] Xiuwen Yi, Yu Zheng, Junbo Zhang, and Tianrui Li. ST-MVL: Filling missing values in geo-sensory time series data. In *Proceedings of the 25th International Joint Conference on Artificial Intelligence*, June 2016.
- [56] Jinsung Yoon, James Jordon, and Mihaela Schaar. GAIN: Missing Data Imputation using Generative Adversarial Nets. In *Proceedings of the 35th International Conference on Machine Learning*, pages 5689–5698. PMLR, July 2018.

## A Theorems and Proof

In the following, we prove the convergence of the GCPG  $\mathbf{Q} = \sigma(\theta)$ .

**Assumption 1** Time-series  $i$  sampled at time  $t$ , denoted as  $x_{i,t} \in \mathbb{R}$  is generated with the Structural Causal Model (SCM), i.e.,  $x_{i,t} = f_i(\mathbf{x}_{1,t-\tau:t-1}, \mathbf{x}_{2,t-\tau:t-1}, \dots, \mathbf{x}_{N,t-\tau:t-1}) + e_{i,t}$ ,  $i = 1, 2, \dots, N$ . Where  $\tau$  denotes the maximal time lag.

**Assumption 2** Component  $i$  of CDNN  $f_{\theta_i}$  approximate generative function  $f_i$  with an error smaller than  $e_{NN,i}$ .

This assumption is satisfied if we leverage the Universal Approximation Theorem of Neural Networks [20]. It is reasonable since we can learn the dynamics under time-series well with our deep neural network.

**Assumption 3**  $\exists \lambda_0, \forall i, j = 1, \dots, N, |f_{\phi_j}(\mathbf{X} \odot \mathbf{s}_{:,j|\mathcal{G}_k=1}) - f_{\phi_j}(\mathbf{X} \odot \mathbf{s}_{:,j|\mathcal{G}_k=0})| > \lambda_0$  if and only if group  $\mathbf{X}_{\mathcal{G}_k}$  Granger cause  $\mathbf{x}_j$ , where  $\mathbf{s}_{:,j|j=r}$  is vector  $\mathbf{s}_{:,j}$  with element  $\mathbf{s}_{ij} = r, \forall i \in \mathcal{G}_k$ .

Here we define  $f_{\phi_j}(\mathbf{X} \odot \mathbf{s}_{:,j}) \triangleq f_{\phi_j}(\{\mathbf{x}_1 \cdot s_{1j}, \dots, \mathbf{x}_N \cdot s_{Nj}\})$  (note that this is not the standard definition of Hadamard product, because  $\mathbf{X}$  is 2-dimensional). This assumption can be regarded as a relaxation of Definition 2, i.e.,

$$|f_j(\{\mathbf{X}_{\mathcal{G}_i}, \mathbf{X} \setminus \mathbf{X}_{\mathcal{G}_i}\}) - f_j(\{\mathbf{0}, \mathbf{X} \setminus \mathbf{X}_{\mathcal{G}_i}\})| \geq \lambda_0 \quad (18)$$

With these assumptions, the grouping version of Theorem 1 in [8] can be formulated as

**Theorem 1** There exists a penalty coefficient  $\lambda$ , s.t. GCPG element  $q_{kj}$  decrease towards 0 if group  $\mathbf{X}_{\mathcal{G}_k}$  does not Granger cause time-series  $j$ ,  $q_{kj}$  increase towards 1 if group  $\mathbf{X}_{\mathcal{G}_k}$  Granger cause time-series  $j$ .

**Proof.** The learned CPG  $\tilde{\mathbf{M}} = \mathbf{G}^T \mathbf{Q}$ , and  $\tilde{\mathbf{m}}_{ij} = \mathbf{g}_{:,i}^T \mathbf{q}_{:,j}$ . Since each time-series is and can only be allocated to one group, we get

$$\mathbf{s}_{:,j} = \mathbf{G}^T \mathbf{s}'_{:,j}, \quad \mathbf{s}'_{:,j} \sim \text{Ber}(\sigma(\theta_{:,j})) \quad (19)$$

The loss function in *Causal Discovery Stage* is

$$\mathcal{L}_{\text{graph}} = \frac{1}{NT} \sum_{j=1}^N \sum_{t=1}^T \|f_{\phi_j}(\mathbf{X} \odot \mathbf{s}_{:,j}) - x_{j,t}\|_2 \cdot o_{j,t} + \lambda \|\sigma(\theta)\|_1 \quad (20)$$

By calculating the gradients of  $\mathbb{E}_{\mathbf{S}} [\mathcal{L}_{\text{graph}}]$  over  $\theta_{ij}$ , we get

$$\frac{\partial}{\partial \theta_{kj}} \mathbb{E}_{\mathbf{S}} [\mathcal{L}_{\text{graph}}] = \frac{1}{NT} \frac{\partial}{\partial \theta_{kj}} \sum_{t=1}^T \mathbb{E}_{\mathbf{S}} \sum_{j=1}^N \|f_{\phi_j}(\mathbf{X} \odot \mathbf{s}_{:,j}) - x_{j,t}\|_2 \cdot o_{j,t} + \lambda \|\sigma(\theta)\|_1 \quad (21)$$

$$= \frac{1}{NT} \sum_{t=1}^T \mathbb{E}_{\{s_{ij}\}_{i \notin \mathcal{G}_k}} \frac{\partial}{\partial \theta_{kj}} \mathbb{E}_{\{s_{ij}\}_{i \in \mathcal{G}_k}} \|f_{\phi_j}(\mathbf{X} \odot \mathbf{s}_{:,j}) - x_{j,t}\|_2 \cdot o_{j,t} + \lambda \sigma'(\theta_{kj}) \quad (22)$$

$$= \frac{1}{NT} \sum_{t=1}^T \mathbb{E}_{\{s_{ij}\}_{i \notin \mathcal{G}_k}} \frac{\partial}{\partial \theta_{kj}} (\sigma(\theta_{kj}) \|f_{\phi_j}(\mathbf{X} \odot \mathbf{s}_{:,j|\mathcal{G}_k=1}) - x_{j,t}\|_2 \cdot o_{j,t} \quad (23)$$

$$+ (1 - \sigma(\theta_{kj})) \|f_{\phi_j}(\mathbf{X} \odot \mathbf{s}_{:,j|\mathcal{G}_k=0}) - x_{j,t}\|_2 \cdot o_{j,t}) + \lambda \sigma'(\theta_{kj}) \quad (24)$$

$$= \frac{1}{NT} \sum_{t=1}^T \mathbb{E}_{\{s_{ij}\}_{i \notin \mathcal{G}_k}} \sigma'(\theta_{kj}) (\lambda + \|e_{NN,i} + e_{t,j}\|_2 \cdot o_{j,t} \quad (25)$$

$$- \|f_{\phi_j}(\mathbf{X} \odot \mathbf{s}_{:,j|\mathcal{G}_k=0}) - x_{j,t}\|_2 \cdot o_{j,t}) \quad (26)$$

$$\approx \frac{1}{NT} \sum_{t=1}^T \mathbb{E}_{\{s_{ij}\}_{i \notin \mathcal{G}_k}} \sigma'(\theta_{kj}) (\lambda + e_{t,j}^2 \cdot o_{j,t} - (\Delta_{\mathcal{G}_k,j} + e_{t,j})^2 \cdot o_{j,t}) \quad (27)$$

$$= \frac{1}{NT} \sum_{t=1}^T \mathbb{E}_{\{s_{ij}\}_{i \notin \mathcal{G}_k}} \sigma'(\theta_{kj}) (\lambda - (2\Delta_{\mathcal{G}_k,j} e_{t,j} + \Delta_{\mathcal{G}_k,j}^2) \cdot o_{j,t}) \quad (28)$$

where  $f_{\phi_j}(\cdot)$  is the MPGNN prediction module,  $\mathbf{s}_{:,j|\mathcal{G}_k=r}$  is generated with (19), only with  $s_{kj} = r$ . And we define  $\Delta_{\mathcal{G}_k,j}$  as the causal effects of group  $\mathcal{G}_k$ , i.e.,

$$\Delta_{\mathcal{G}_k,j} = f_{\phi_j}(\mathbf{X} \odot \mathbf{s}_{:,j|\mathcal{G}_k=1}) - f_{\phi_j}(\mathbf{X} \odot \mathbf{s}_{:,j|\mathcal{G}_k=0}) \quad (29)$$

We achieve (21) by changing the order of summation, (22) by eliminating irrelevant terms in CDNN and splitting the summation of  $s_{ij}$  where  $i$  is in or not in group  $\mathcal{G}_k$ , (23, 24) by calculating the expectation of Bernoulli distribution, (26) by ignoring  $e_{NN,j}$ . When we treat observation mask  $o_{jt}$  and noise  $e_{jt}$  as random variables, we get the expectation of the derivatives

$$\mathbb{E}_{o_{jt}} \mathbb{E}_{e_{jt}} \frac{\partial}{\partial \theta_{kj}} \mathbb{E}_{\mathbf{S}} [\mathcal{L}_{\text{graph}}] = \frac{1}{NT} \sum_{t=1}^T \mathbb{E}_{\{s_{ij}\}_{i \notin \mathcal{G}_k}} \mathbb{E}_{o_{jt}} \mathbb{E}_{e_{jt}} \sigma'(\theta_{kj}) (\lambda - (2\Delta_{\mathcal{G}_k,j} e_{t,j} + \Delta_{\mathcal{G}_k,j}^2) \cdot o_{j,t}) \quad (30)$$

$$= \frac{1}{NT} \sum_{t=1}^T \mathbb{E}_{\{s_{ij}\}_{i \notin \mathcal{G}_k}} \sigma'(\theta_{kj}) (\lambda - \Delta_{\mathcal{G}_k,j}^2 \cdot p) \quad (31)$$

Where  $p$  is the missing probability.  $\sigma'(\cdot)$  is the derivative of the sigmoid function and is always positive.

If group  $\mathcal{G}_k$  does not Granger cause  $j$ , then  $|\Delta_{\mathcal{G}_k,j}| < \lambda_0$  (Assumption 3). Then setting  $\lambda = p\lambda_0^2$  would make (31) expected to be positive, and  $\theta_{kj}$  decreases towards  $-\infty$ ,  $q_{kj} = \sigma(\theta_{kj})$  decreases towards 0. Similarly, If group  $\mathcal{G}_k$  Granger cause  $j$ , (31) is expected to be negative and  $q_{kj} = \sigma(\theta_{kj})$  increases towards 1.

## B Additional Experiments

### B.1 Imputation Performance

**Related Works for Time-series Imputation.** Imputation of missing entries is a significant problem in the field of multivariate time-series analysis. There exists a large amount of imputation

Table 4: Imputation performance on AQI dataset in terms of MSE. Performance in terms of MAPE is shown in Tab. 5. Note that GRIN uses a geometric distance graph while the other approaches do not.

Met.	AQI with RM		AQI with RBM	
	$p = 0.3$	$p = 0.6$	$p_{\text{blk}} = 0.15\%$	$p_{\text{blk}} = 0.3\%$
Mean	498.77 $\pm$ 3.18	501.61 $\pm$ 1.59	496.21 $\pm$ 7.99	498.94 $\pm$ 7.92
KNN	147.84 $\pm$ 18.50	175.72 $\pm$ 16.53	162.02 $\pm$ 3.91	169.60 $\pm$ 13.07
Soft	211.63 $\pm$ 1.74	234.78 $\pm$ 11.01	206.04 $\pm$ 2.17	205.89 $\pm$ 10.46
BRITS	118.91 $\pm$ 1.43	165.65 $\pm$ 0.00	129.64 $\pm$ 8.96	137.44 $\pm$ 5.58
CGCNImp	283.54 $\pm$ 27.03	374.03 $\pm$ 4.22	283.88 $\pm$ 13.82	305.48 $\pm$ 14.96
TimesNet	149.55 $\pm$ 1.87	228.40 $\pm$ 3.47	155.75 $\pm$ 11.16	163.72 $\pm$ 9.83
GRIN	70.16 $\pm$ 1.49	106.57 $\pm$ 3.96	101.07 $\pm$ 9.04	<b>120.29 <math>\pm</math> 7.06</b>
CUTS+	<b>64.55 <math>\pm</math> 2.14</b>	<b>96.11 <math>\pm</math> 4.41</b>	<b>97.67 <math>\pm</math> 3.91</b>	127.39 $\pm$ 8.62

Table 5: Imputation performance on AQI dataset in terms of MAPE.

Met.	AQI with RM		AQI with RBM	
	$p = 0.3$	$p = 0.6$	$p_{\text{blk}} = 0.15\%$	$p_{\text{blk}} = 0.3\%$
Mean	0.8674 $\pm$ 0.0024	0.8775 $\pm$ 0.0070	0.8475 $\pm$ 0.0050	0.8590 $\pm$ 0.0074
KNN	0.2475 $\pm$ 0.0191	0.2860 $\pm$ 0.0215	0.2592 $\pm$ 0.0032	0.2723 $\pm$ 0.0111
Soft	0.3148 $\pm$ 0.0019	0.3357 $\pm$ 0.0099	0.3077 $\pm$ 0.0030	0.3091 $\pm$ 0.0054
BRITS	0.2742 $\pm$ 0.0047	0.3885 $\pm$ 0.0150	0.2757 $\pm$ 0.0034	0.2832 $\pm$ 0.0054
CGCNImp	0.6206 $\pm$ 0.0419	0.7304 $\pm$ 0.0074	0.6286 $\pm$ 0.0140	0.6526 $\pm$ 0.0102
TimesNet	0.3491 $\pm$ 0.0104	0.4933 $\pm$ 0.0111	0.3431 $\pm$ 0.0128	0.3503 $\pm$ 0.0154
GRIN	0.1891 $\pm$ 0.0107	0.2950 $\pm$ 0.0334	0.2328 $\pm$ 0.0056	<b>0.2583 <math>\pm</math> 0.0112</b>
CUTS+	<b>0.1559 <math>\pm</math> 0.0046</b>	<b>0.2314 <math>\pm</math> 0.0108</b>	<b>0.2248 <math>\pm</math> 0.0119</b>	0.2649 $\pm$ 0.0140

approaches. For example, *KNN-based methods* that reconstruct the missing values with k-nearest neighbors [4, 47]. *Autoregressive-based methods* that perform imputation by fitting a parameterized model [13]. Methods based on *Low-rank-approximation* [16, 15]. And *Chain-equation-based methods* (or MICE) [1, 48, 50] that estimates missing values with iterative series of predictive models.

Recently, time-series imputation is more explored with the emerging Neural Networks (NNs). Recurrent NNs (RNNs) is most used in this line of research. For example, Cao et al. [6] proposed BRITS to directly learn the missing values in dynamic systems without specific assumptions. Other researches include [7, 26, 40, 27]. Other than RNNs, Luo et al. [31] and Yoon et al. [56] proposed to generate realistic reconstructed values with Generative Adversarial Networks (GANs). Wu et al. [52] imputes missing entries by capturing the multi-periodicity in time-series with 2D Convolutional-NNs and Fast Fourier Transform. Cini et al. [10] further propose GNN(Graph NNs)-based methods for processing high-dimensional sequential data, since GNNs are expressive and scalable tools for multivariate time-series analysis [25]. The graph used in [10] are built using available relation information, e.g., geometric distance. However, in most real applications, the ground truth relational graph is not known a priori. In CUTS+, we use the discovered causal graph instead.

**Baseline Algorithms.** We compared our method with 7 baseline algorithms: (i) Mean imputation, which replaces missing entries with the mean value of each column; (ii) KNN imputation, making use of the nearest neighbor imputations to estimate missing values based on the mean squared difference on features; (iii) SoftImpute, a matrix completion by iterative soft thresholding of SVD decompositions [32]. (iv) BRITS [6], based on bidirectional recurrent neural networks; (v) TimesNet [52], which transforms the 1D time series into a set of 2D tensors based on multiple periods modeled by 2D kernels; (vi) CGCNImp [28], based on two related modules, one using GCN to learn Granger causality, and the other relying on attention-driven LSTM to learn time series dependencies; (viii) GRIN [10], a method using graph-based neural networks by exploiting information coming from sensors at different locations. The (i, ii, iii) approaches are implemented by `fancyimpute`, a Python library of imputation algorithms.

**Dataset.** To demonstrate the performance of our method on large-scale datasets, we use air quality (AQI) dataset <sup>4</sup>. Air Quality is a dataset of several air quality features (such as PM2.5, SO<sub>2</sub>,

<sup>4</sup><https://www.microsoft.com/en-us/research/project/urban-computing/>

NO<sub>2</sub>) from 437 monitoring stations spread across 43 Chinese cities, with an hourly measurement over a period of one year. We consider PM2.5 pollution index in the dataset, which has minimal missing values among all the features. Those 437 stations can be divided into two parts, respectively distributed in City Cluster A centered around Beijing and City Cluster B centered around Shenzhen. Here we only use the Cluster B part centered around Shenzhen, which has a lower variance. The total length of the dataset is  $L = 8760$  and the number of nodes is  $N = 163$ .

**Results.** Experiments in Tab. 4 and 5 show that CUTS+ achieve high imputation performance on AQI dataset with 4 missing data scenarios. Compared with the state-of-the-art, we beat all other approaches with RM. With RBM, we beat TimesNet and CGCNImp, only GRIN slightly outperforms us. However, GRIN uses a geometric distance graph while our approach achieves a similar or better performance than GRIN without a geometric graph. This proves that our approach does discover reliable causal graphs with time-series and the imputation performance is largely enhanced.

## B.2 More Scalability Experiments

In Section 5.1 we show the scalability of our CUTS+ on VAR and Lorenz-96 datasets. We show more experiments on VAR and Lorenz-96 with  $N = 16, 32, 64, 128, 256, 512$  on 2 different data missing scenarios. The results are in Tab. 6. We observe good scalability when  $N$  increases.

Table 6: Performance comparison of CUTS+ on VAR and Lorenz-96 datasets with  $N = 32, 128, 512$ . The missing is set as RM with  $p = 0.3$ .

$N$	VAR with RM		Lorenz-6 with RM	
	$p = 0.3$	$p = 0.6$	$p = 0.3$	$p = 0.6$
16	0.9975 ± 0.0003	0.9929 ± 0.0021	1.0000 ± 0.0000	0.9578 ± 0.0080
32	1.0000 ± 0.0000	0.9989 ± 0.0007	0.9938 ± 0.0014	0.9790 ± 0.0035
64	0.9999 ± 0.0001	0.9988 ± 0.0010	0.9901 ± 0.0015	0.9689 ± 0.0045
128	0.9866 ± 0.0009	0.9795 ± 0.0019	0.9915 ± 0.0034	0.9640 ± 0.0018
256	0.9917 ± 0.0027	0.9836 ± 0.0047	0.9951 ± 0.0003	0.9773 ± 0.0041
512	0.9866 ± 0.0038	0.9553 ± 0.0133	0.9964 ± 0.0006	0.9868 ± 0.0010

## C Implementation Details

### C.1 Compute

We conduct experiments on a PC with Intel Core CPUs and NVIDIA GeForce RTX 3090 GPUs. The total computation process for CUTS+ takes fewer than 5 hrs. For baseline algorithms such as PCMC and LCCM, the computation time is extremely long when  $N \geq 128$  (more than 12 hrs each task), so we only perform comparisons with PCMC and LCCM on NetSim and Dream-3 datasets.

### C.2 Datasets

The VAR and Lorenz-96 datasets support setting  $N$ . To ensure the numbers of causal parents for each time-series in VAR are roughly the same when  $N$  changes, the sparsity of the causal matrix is set as 0.2, 0.1, 0.05, 0.03, 0.015, 0.008 for  $N = 16 \sim 512$ , respectively.

The 4 data missing scenarios used in the experiments are RM ( $p = 0.3/0.6$ ) and RBM ( $p_{\text{blk}} = 0.15\%/0.3\%$ ). We list the detailed parameter settings in Tab. 7.

Table 7: Parameter settings for our 4 types of data missing.

Setting	$p$	$p_{\text{blk}}$	$L_{\min}$	$L_{\max}$
RM $p = 0.3$	0.3	0	/	/
RM $p = 0.6$	0.6	0	/	/
RBM $P_{\text{blk}} = 0.15\%$	0.1	0.0015	12	48
RBM $P_{\text{blk}} = 0.3\%$	0.1	0.003	12	48

### C.3 CUTS+

We show the key parameters of CUTS+ in Tab. 8 and discuss some details for implementation in the following.

**C2FD.** During the Course-to-fine Causal Discovery (C2FD) process, we choose the initial number of groups based on the nodes of the data. After every 20 epochs, the number of groups doubles, and a probability graph is generated based on the new number of groups.

**Sliding Window Imputation.** For every batch, we extract data from a defined temporal interval. Then, we perform predictions at each temporal point by iteratively utilizing previously gathered data. To handle data from the initial temporal points without certain precious time points, a learnable parameter within the CUTS+ network is configured to derive an initial hidden state, which serves as the replacement for the unattainable predecessor data.

**Early Stopping.** To mitigate the overfitting of the network, the training process is terminated if the performance metric does not improve within a specified epoch. Once the optimal number of epochs on the validation set is determined in the context of causal inference, the causal graph can be relearned using this number on the test set.

### C.4 Baseline Methods

This work incorporates a lot of baseline methods. We briefly describe the implementation details for reproducibility in the following and show key parameters in Tab. 9.

**PCMCI.** The code is from <https://github.com/jakobrunge/tigramite>. We use ParCorr as conditional independence tests for all experiments. Although nonlinear tests, e.g., CMIKnn, and GPDC are available, but the computational cost is unacceptable for our high-dimensional settings.

**NGC.** The code is from <https://github.com/iancovert/Neural-GC>. We use the cMLP network because according to the original paper [46] cMLP achieves better performance, except for DREAM-3 dataset.

**eSRU.** The code is from [https://github.com/sakhanna/SRU\\_for\\_GCI](https://github.com/sakhanna/SRU_for_GCI).

**SCGL.** The code is downloaded from link shared in its original paper [53].

**LCCM.** The code is from <https://github.com/edebrouwer/latentCCM>.

**NGM.** The code is from <https://github.com/alexisbellot/Graphical-modelling-continuous-time>.

**CUTS.** The code is from <https://github.com/jarrycyx/UNN>. In the ablation study, we add C2FD to CUTS, named ‘‘CUTS w C2FD’’.

**BRITS.** The code is from <https://github.com/caow13/BRITS>.

**CGCNImp.** The code is from <https://github.com/zhewen166/CGCNImp>.

**TimesNet.** The code is from <https://github.com/thuml/TimesNet>.

**GRIN.** The code is from <https://github.com/Graph-Machine-Learning-Group/grin>.

**Fancyimpute.** We implement Mean imputation, KNN Imputation, and Soft Imputation with fancyimpute. The code is from <https://pypi.org/project/fancyimpute/>.

Table 8: Hyperparameters settings of CUTS+ in the aforementioned experiments. The number of nodes in VAR and Lorenz dataset is 512.

Hyperparam.	VAR	Lorenz	NetSim	DREAM-3	AQI
Batch size	32	32	32	32	16
Window size	16	8	8	24	24
Initial groups	128	32	/	25	10
Weight decay	0	0	0	0.0001	0
Stage 1 Lr	$10^{-5} \rightarrow 10^{-6}$	$10^{-3} \rightarrow 10^{-4}$	$10^{-4} \rightarrow 10^{-5}$	$10^{-3} \rightarrow 10^{-4}$	$10^{-3} \rightarrow 10^{-4}$
Stage 2 Lr	$10^{-2} \rightarrow 10^{-3}$	$10^{-4} \rightarrow 10^{-5}$	$10^{-3} \rightarrow 10^{-4}$	$10^{-4} \rightarrow 10^{-5}$	$10^{-2} \rightarrow 10^{-3}$
Gumbel $\tau$	$5 \rightarrow 0.5$	$5 \rightarrow 0.5$	$5 \rightarrow 0.5$	$5 \rightarrow 0.5$	$1 \rightarrow 0.1$
$\lambda$	$0.05 \rightarrow 0.005$	$0.05 \rightarrow 0.005$	$0.2 \rightarrow 0.02$	$0.2 \rightarrow 0.02$	$1 \rightarrow 0.1$

Table 9: Hyperparameters settings of the baseline causal discovery and data imputation algorithms.

Methods	Params.	VAR	Lorenz	NetSim	DREAM-3
PCMCI	$\tau_{max}$	3	3	5	5
	$PC_{\alpha}$	0.05	0.05	0.05	0.05
NGC	Learning rate	0.05	0.05	0.05	0.05
	$\lambda_{ridge}$	0.01	0.01	0.01	0.01
	$\lambda$	0.02 $\rightarrow$ 0.2	0.02 $\rightarrow$ 0.2	0.04 $\rightarrow$ 0.4	0.02 $\rightarrow$ 0.01
eSRU	$\mu_1$	0.1	0.1	0.1	0.7
	Learning rate	0.01	0.01	0.001	0.001
	Batch size	250	250	100	100
	Epochs	2000	2000	2000	2000
SCGL	Epochs	50	50	50	50
	Batch size	32	32	32	32
	Window	3	3	3	3
LCCM	Epochs	50	50	50	50
	Batch size	10	10	10	10
	Hidden size	20	20	20	20
NGM	Steps	2000	2000	2000	2000
	Horizon	5	5	5	5
	GL_reg	0.05	0.05	0.05	0.05
	Chunk num	100	100	100	46
CUTS	$n_1$	5	50	200	20
	$n_2$	15	150	600	30
	$n_3$	30	300	200	50
	$\alpha$	0.1	0.01	0.01	0.01
	Input step	3	1	5	5
	Batch size	128	128	128	128
	Hidden features	128	128	128	128
	Network layers	3	3	3	5
	Weight decay	0.001	0	0.001	0
	Stage 1 Lr	$10^{-4} \rightarrow 10^{-5}$	$10^{-4} \rightarrow 10^{-5}$	$10^{-4} \rightarrow 10^{-5}$	$10^{-4} \rightarrow 10^{-5}$
	Stage 2 Lr	$10^{-2} \rightarrow 10^{-3}$	$10^{-2} \rightarrow 10^{-3}$	$10^{-2} \rightarrow 10^{-3}$	$10^{-2} \rightarrow 10^{-3}$
Gumbel $\tau$	1 $\rightarrow$ 0.1	1 $\rightarrow$ 0.1	1 $\rightarrow$ 0.1	1 $\rightarrow$ 0.1	
$\lambda$	0.1	0.1	5	5	

## D Broader Impacts

This work takes into account the high-dimensionality problem which is seldomly focused on by previous works. CUTS+ paves the way toward causal discovery in real applications in which the time-series often contain hundreds of variables. The possible application fields include medicine, healthcare, social science, and finance.

## E Limitations

Our approach, CUTS+, is a Granger-causality-based causal discovery algorithm. A main limitation of our CUTS+ is the gap between Granger causality and real causality. Granger causality may fail when there exists latent confounders or sub-sampled causal effects, which are common in real datasets. Moreover, our CUTS+ handle irregular time-series with missing data imputation module and cannot directly use irregular inputs. The performance may be hampered when the sampling frequency of each time-series is different.